

Dynamics of Multifragmentation in Heavy Ion Collisions

Willibrord. REISDORF¹

*Gesellschaft für Schwerionenforschung (GSI)
Postfach 110552, D-64220 Darmstadt, Germany*

Abstract

We review multifragmentation data obtained at the SIS/GSI accelerator using heavy ion beams with (0.1-1)A GeV together with the ALADIN and FOPI experimental setups.

1 Introduction

Multifragmentation, that is the emission of several intermediate mass fragments from a hot nucleus, is a phenomenon observed in nuclear reactions, using light and heavy projectiles over a wide incident energy range. Besides the scientific curiosity to understand what happens, some of the hopes in these studies are that one can learn more about the tendency of fermionic nuclear matter to appear in clusters and, perhaps eventually, about the topology of the nuclear phase diagram, in particular the evasive liquid-to-gas transition and, from the explosive features of some of the reactions, about nuclear matter compressibility. Such information is of high interest in other fields as well, such as astrophysics. As the underlying mechanisms are likely to be rather complex, statistical approaches have been invoked from the beginning in order to try to understand the experimental data. Evidence for non-equilibrium effects have lead to the parallel development of sophisticated transport models as well.

As this written contribution represents essentially the contents of a one-hour lecture, it is highly limited in scope: I describe experimental multifragmentation data measured in the past years at GSI, Darmstadt (Germany). The many facets of multifragmentation are studied in laboratories all over the world, however. I refer the reader to a recent workshop [1] on Multifragmentation for more encompassing information on this subject.

I shall start by describing the ALADIN and FOPI experimental setups and the way observed multiparticle events are sorted. Then I review fragment yield distributions in both central and peripheral collisions together with attempts to derive from them apparent chemical temperatures. Detailed information on momentum space distributions will allow me to discuss subjects such as the determination of the caloric curve, the influence of flow and the system-size dependence. Finally, an isospin tracer experiment, performed to study the degree of equilibration, will be described.

¹ E-mail address: W.Reisdorf@gsi.de

2 Apparatus

Two large detection systems have been set up at the heavy ion synchrotron SIS at GSI Darmstadt, ALADIN (Fig. 1) and FOPI (Fig. 2).

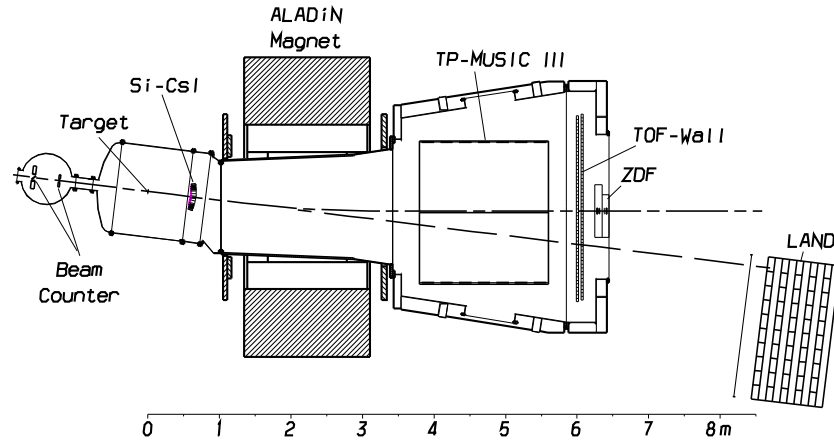


Figure 1: Schematic view of the ALADIN spectrometer in the bending plane [4].

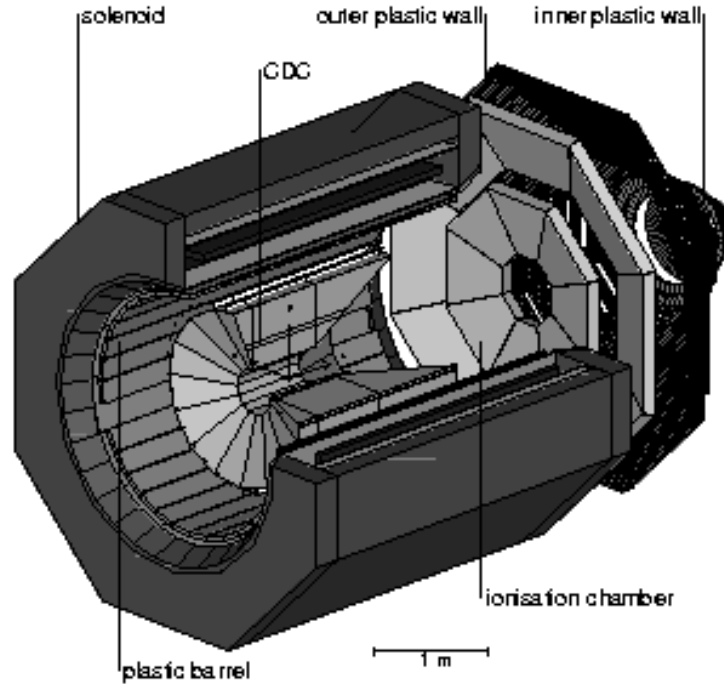


Figure 2: Schematic view of the FOPI detector.

The ALADIN [4] spectrometer was designed primarily to look at fast projectile-like spectator fragments focussed into a forward cone of about $\pm 5^\circ$. The core of the apparatus consists of a magnet operated at a bending power of 1.4 Tm, a time projection multiple-sampling ionization chamber TP-MUSIC and a time-of-flight (TOF) wall. In some experiments complementary detectors are installed, such as a large area neutron detector LAND that identifies neutrons emitted close to 0° , and a series of multidetector hodoscopes consisting of Si-Cs(Tl) telescopes, CaF_2 plastic phoswich detectors and Si-strip detectors arranged so as to cover angles between $6 - 58^\circ$. One of the purposes of the TP-MUSIC detector is to allow precise tracking of charged particles passing through its active volume. The version MUSIC-II [6] is shown in Fig. 3.

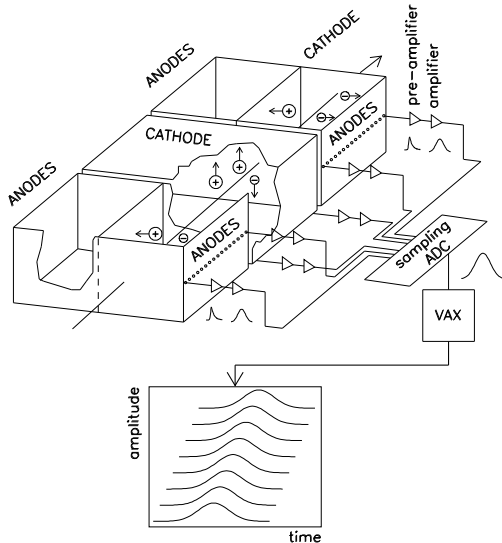


Figure 3: Illustration of the operation of the MUSIC II detector From ref. [6]

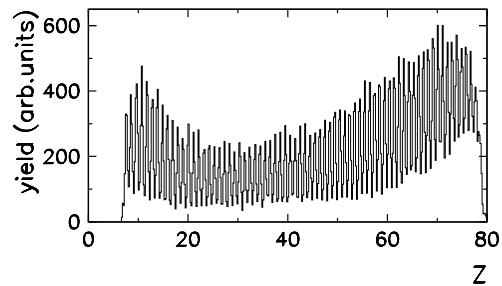


Figure 4: Observed charge spectrum. From ref. [6]

It consists of three active volumes with the electric drift fields in adjacent sections perpendicular to each other, two for the measurement of the horizontal and one for that of the vertical position and angle of the particle track. To allow multiple sampling of the particle signals, each anode is subdivided into 16 stripes with a width of 3 cm each. The anode signals are recorded using flash analog-to-digital converters (ADCs) with a sampling rate of 16 MHz. Better than unit resolution for nuclear charges from $Z=8$ all the way to Au ($Z=79$) is obtained (Fig. 4). Charges between $Z=2$ and 15 can be resolved with use of the scintillator strips in the TOF.

The FOPI apparatus was built to study central heavy ion reactions in the energy range 0.1-2A GeV. Particle identification, again, is done by a combined energy-loss, time-of-flight and magnetic rigidity analysis. The magnet

is a superconducting solenoid operated at 0.6 T (see Fig. 2). Time of flight and energy-loss are determined by about 1000 scintillator detectors arranged octagonally in the downstream part of the detector (PLASTIC WALL) and as a barrel inside the magnet. At lower incident energies ($E/A \leq 400$ MeV) a set of gas ionization chambers is inserted in front of the PLASTIC WALL to allow identification of slower heavy clusters (up to Z about 15). Inside the magnet, the particles are tracked in drift chambers, the Central Drift Chamber, CDC, and the HELITRON (usually installed in front of the CDC, but not shown here). Fig. 5 allows to visualize individual particle tracks in a specific event determined with use of local or global (Hough transform) track finding methods.

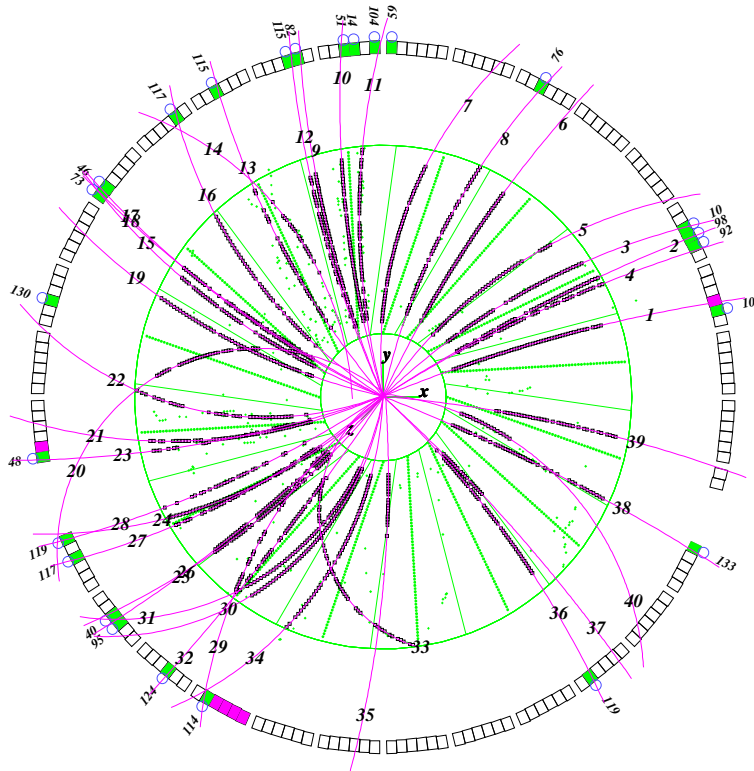


Figure 5: Event display in the Central Drift Chamber. A cross section in the plane perpendicular to the beam axis is shown

By matching these tracks to the outer barrel scintillators one obtains the energy loss (from the ionization in the CDC gas), the track curvature and the time-of-flight (from the Barrel). Fig. 6 shows well separated pions , protons, deuterons and tritons.

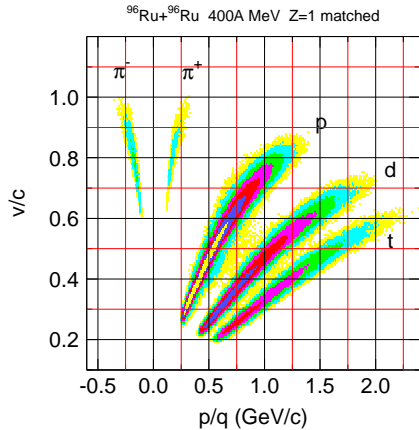


Figure 6: Identification of charge-one particles in the velocity versus magnetic rigidity plane

3 Event sorting

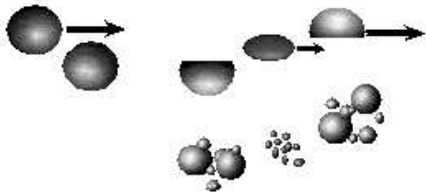


Figure 7: Evolution of a heavy ion collision: spectators and participants

Heavy ion collisions lead to events with very different topologies. It is highly desirable to sort these events according to some criteria, such as the impact parameter b . As b itself cannot be measured directly one tries to find an observable that is believed to be strongly correlated to b . The methods used by both ALADIN and FOPI are easiest to visualize in the participant-spectator picture illustrated in Fig. 7. In experi-

ments with the ALADIN spectrometer one selects impact parameters by measuring the size of the projectile spectator: one adds up the charges of all the fragments with $Z > 1$ moving forwards in a narrow rapidity window, see Fig. 8. This sum has been dubbed Z_{bound} : large Z_{bound} obviously correspond to rather peripheral collisions. In experiments with the FOPI detector which are primarily performed to study fireball (participant) physics, a standard method is to determine the charged-particle multiplicity. The underlying idea is that 'fireball matter' emits more particles than 'spectator matter'. In the early phase of running the detector the multiplicity, PM, observed in the PLASTIC WALL, which covers only laboratory angles forwards of 30° , was taken. Due to this geometric limitation, overcome later when the full detector became available, other more powerful methods to 'maximize' the fireball (i.e. choosing very central collisions) were developed. Fig. 9 illustrates the increasingly 'compact' momentum space topology of $Z=4$ fragments emitted in Au on Au reactions at 250A MeV as selection is done, first, according to high Plastic Wall

multiplicities PM (lower panel, where still spectator peaks are visible), second, according to large 'ERAT', the ratio of total transverse to longitudinal kinetic energies (center panel) and finally, using large ERAT and low directivity, i.e. high azimuthal symmetry. The directivity is obtained from $\sum \omega Z \vec{u}_t / \sum Z |u_t|$ ($\omega = \pm 1$ forward/backward, Z fragment charge, \vec{u}_t transverse 4-velocity). In the figure both the rapidity (abscissa) and the transverse 4-velocity (ordinate) are scaled with the respective projectile values, placing the midrapidity value at zero. The ERAT and PM selections correspond to cross sections of 200 mb, the additional low-directivity condition cuts the cross section down to 70 mb. For more details see [9].

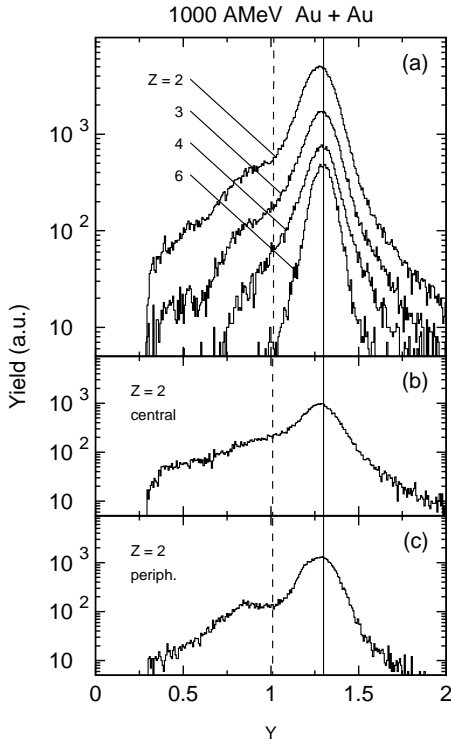


Figure 8: (a): Rapidity spectra measured in the reaction Au+Au at 1000A MeV for fragments with $Z=2,3,4$ and 6. (b): Rapidity spectra for $Z=2$ fragments in central collisions and (c): in peripheral collisions. From ref. [4]

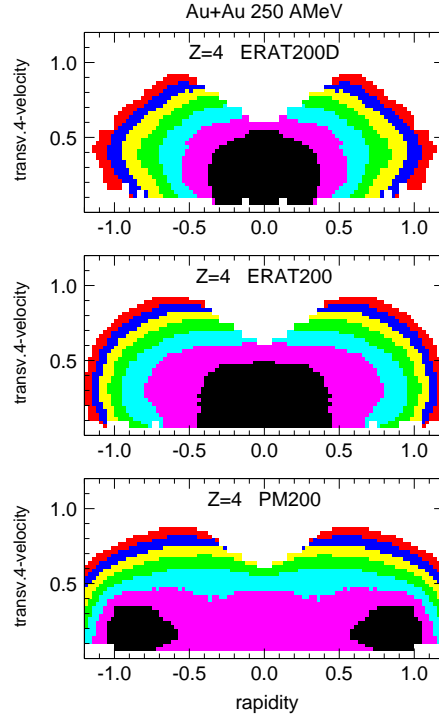


Figure 9: Invariant cross section contour plots (scaled units) for Be ($Z=4$) fragments observed in the system Au+Au at 250A MeV. The three panels correspond to different event selections, see text. From ref. [9]

4 Cluster production: peripheral and central collisions. Universality.

Multifragment decays of projectile-spectator sources have been studied extensively with the ALADIN spectrometer. [2] - [8] One of the hopes was that spectator matter would be 'gently' excited, initially uncompressed nuclear matter, that would equilibrate relatively fast, then expand slowly under heat pressure and enter into the unstable spinodal regime where its decay would show features of a liquid-to-vapour transition. Evidence that multifragmentation was a phenomenon following complete equilibration was obtained by the observed 'universality' of the decay pattern. As shown in Fig. 10, if one plots the observed mean multiplicity of intermediate mass fragments (IMF, $Z = 3 - 30$) against the size of the spectator charge, characterized by Z_{bound} , (i.e. against the impact parameter for a fixed target-projectile system), one finds a dependence that remains invariant against the variation of the incident energy. [4]

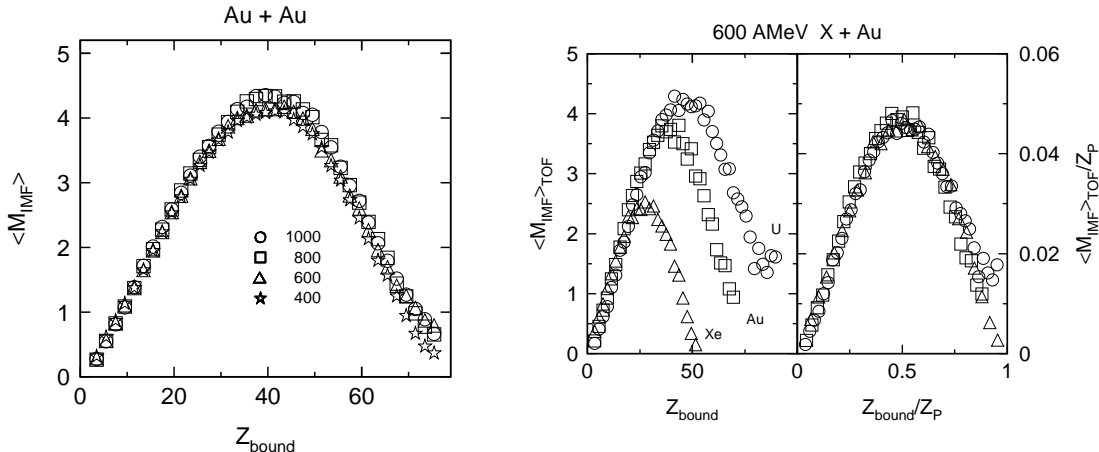


Figure 10: (a): Mean multiplicity of intermediate mass fragments as a function of Z_{bound} for the reaction Au+Au at $E/A = 400, 600, 800$ and 1000 MeV. [4]

Figure 11: Left panel: Mean multiplicity of intermediate mass fragments as a function of Z_{bound} for the reactions ^{238}U on ^{197}Au (circles), ^{197}Au on ^{197}Au (squares) and ^{129}Xe on ^{197}Au (triangles) at $E/A = 600$ MeV. Right panel: the same data after normalizing both quantities with respect to the atomic number Z_p of the projectile. [4]

Other observables characterizing the population of partition space were found to be 'universal' as well. Provided the projectile beam (Au) was not changed, universality was not lost when the Au target was replaced by lighter target materials, all the way down to Be. Further 'ALADIN plots', obtained by fixing the target to Au, but varying this time the size of the projectile

from U down to Xe (left panel Fig. 11), are again merged into one curve when scaling the IMF multiplicity with the projectile size (right panel Fig. 11).

The independence of fragment charge distributions on the size of the source could also be observed in central fusion-like reactions at lower incident energies using the 4π multidetector INDRA at the GANIL accelerator, Caen, France, see Fig. 12. [10] Studying the systems $^{129}\text{Xe}+\text{Sn}$ at 32A MeV and $^{238}\text{U}+^{155}\text{Gd}$ at 36A MeV, it was found that the charge distributions for fragments with charge $Z > 4$ were essentially identical, if scaled with the system size, or, as done in the figure, with the average multiplicity of charged particles with $Z > 4$ (the ratio of the latter is close to the ratio of the system sizes). It was argued in ref. [10] that the available excitation energy, 7A MeV, was the same for both systems.

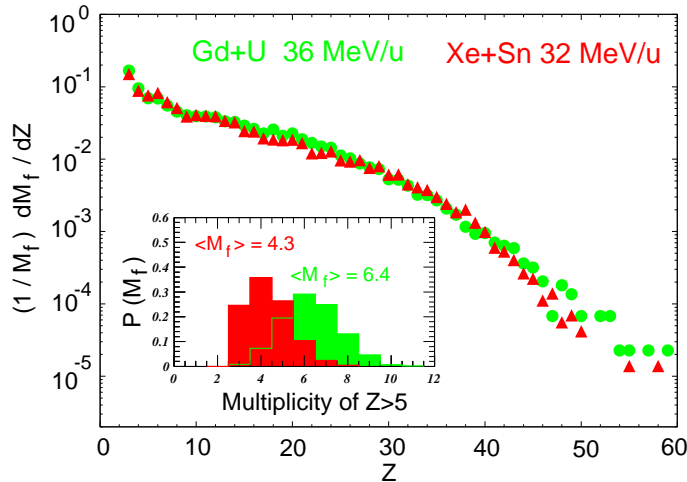


Figure 12: Charge distributions in the reactions Gd+U at 36A MeV (circles) and Xe+Sn at 32A MeV (triangles). Insert: Multiplicity distributions for fragments with $Z \geq 5$ in the same systems. After ref. [10]

Beaulieu et al. [11] pointed out earlier that the excitation energy per nucleon was the relevant parameter for sorting out multifragmentation data. In Fig. 13 the authors show evidence for scaling of system-size normalized IMF multiplicity data, when plotting them against the excitation energy per nucleon: quasi-projectile decay data for the reactions $^{35}\text{Cl}+^{197}\text{Au}$ at 43A MeV and $^{70}\text{Ge}+\text{Ti}$ at 35A MeV are shown together with ALADIN spectator decay data in the reaction Au+Au at 600A MeV. The non-trivial determination of the excitation energy deposited into the presumably thermalized part of the system will be discussed in the next section. As pointed out in ref. [11] there is an important difference between 'quasi-projectile' data ($E/A < 50$ MeV) and 'projectile-spectatator' data ($E/A \geq 600$ MeV): in the former case the average mass of the emitting sources is almost constant due to total-charge

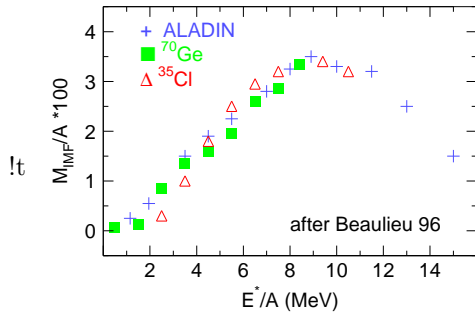


Figure 13: Average number of intermediate mass fragments (scaled by the system size) as a function of the excitation energy per nucleon. Triangles: $^{35}\text{Cl} + ^{197}\text{Au}$ at 43A MeV, squares: $^{70}\text{Ge} + \text{Ti}$ at 35A MeV, crosses: ALADIN data. After ref. [11]

requirements in the experiment, whereas in the latter case the Au projectile spectator decreases from mass $A \sim 190$ to $A \sim 50$ over the excitation energy range in the figure.

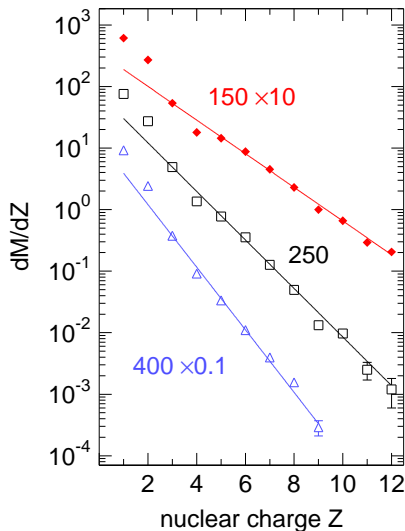


Figure 14: Charge distributions in central collisions of Au on Au at 150, 250 and 400A MeV. [9]

Before closing this section, let us briefly present the 'fireball' part of the story. [9] In very central Au on Au collisions above 100A MeV one finds almost perfectly exponential charge distributions (Fig. 14), the slope merely becoming steeper as the excitation energy is raised. As shown in the Fig. 15, the probability for a proton to appear attached to at least one other nucleon decreases rather slowly from about 80% at 200A MeV to still 50% at 1A GeV. As in these energies the 'available' c.o.m. energies are well beyond typical nucleon binding energies, dynamic mechanisms, such as cooling by adiabatic expansion, or non-equilibrium processes must be invoked to explain such high degrees of clusterization.

5 Chemical temperatures

Frequently 'Statistical Multifragmentation Models' (SMM) are used to compare with data under the assumption of at least chemical equilibrium. The physics input involved are degrees of freedom of hot liquid drops modeled in analogy to the Weizsäcker formula for cold nuclei, a more or less extended list of known discrete levels and some global level density formula to extrapolate to unresolved continuum excited states. Subtle sampling methods (within the

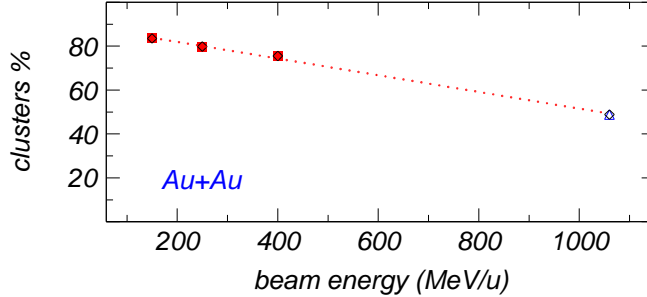


Figure 15: Degree of clusterization (%) of protons in central Au on Au collisions.

grand-canonical, canonical or even microcanonical framework) allow one then to dial typical 'events' under the minimal assumption of basically homogeneous available phase space population. Before being able to compare with experiment the 'primordial' fragment distribution has to be corrected for later sequential decays and the adiabatic pickup of potential field energy prevalent at the moment of 'freeze out'. (Usually only the Coulomb part is taken into account). Comparison of one such model [13, 14] with the ALADIN data is shown in Figs. 16, 17, 18 taken out of the thesis work [8] of T. Odeh. Typically, one assumes freeze out at a nucleon density $\rho = 1/3\rho_0$ (ρ_0 is the saturation density), and adjusts the excitation energy (which such static theories cannot predict) until the data are reproduced. As the ALADIN curve must come down to zero at the left end because of reaching zero spectator size, as well as at the right end (high values of Z_{bound}) because grazing collisions do not lead to any sizeable excitation, there is sensitivity to the theory, and in particular to the assumed excitation energy, only for intermediate Z_{bound} values. Excitation energies of about 4, resp. 10 MeV per nucleon are deduced for spectator nuclei with masses 160, resp. 40. Once the ALADIN curve is reproduced, (upper panel Fig. 16), one finds that other observables characterizing partition space are reproduced as well: see for instance the lower panel of Fig. 16 where the asymmetry parameter $a_{12} = (Z_{max} - Z_2)/(Z_{max} + Z_2)$ is plotted (Z_{max} and Z_2 are the largest and next-to-largest fragment charges).

The chemical temperature deduced from the model is displayed in Fig. 17 and turns out to be rather flat in the Z_{bound} range where there is sensitivity to the data adjustment. A well known method [15] to obtain density-independent temperatures consists in evaluating double isotope yield ratios, such as $({}^6\text{Li}/{}^7\text{Li}) / ({}^3\text{He}/{}^4\text{He})$. The deduced temperature, dubbed $T(\text{HeLi})$, corrected for sequential decays, is also plotted in Fig. 17 together with that deduced from the statistical model applying to it the same treatment as to the isotope data. The remarkable consistency of these apparent temperatures has to be confronted, however, with the failure of the model to predict correctly

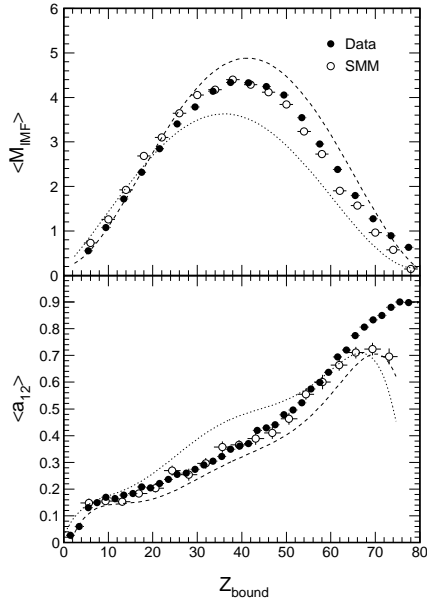


Figure 16: Average intermediate mass fragment multiplicity (upper panel) and average charge asymmetry (lower panel) as a function of Z_{bound} for experiment (full dots) and statistical multifragmentation theory (open dots). The dotted and dashed curves show the model sensitivity to a $\pm 15\%$ variation of the excitation energy. [8]

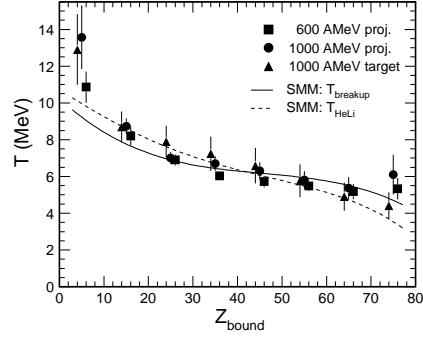


Figure 17: The temperature $T(\text{HeLi})$ as a function of Z_{bound} . Both projectile (600 and 1000A MeV) and target (1000A MeV) spectator data are given. The dashed line represents $T(\text{HeLi})$ as determined with use of the statistical model and the full line gives the model's breakup temperature. [8]

the ratios of the hydrogen isotopes, Fig. 18.

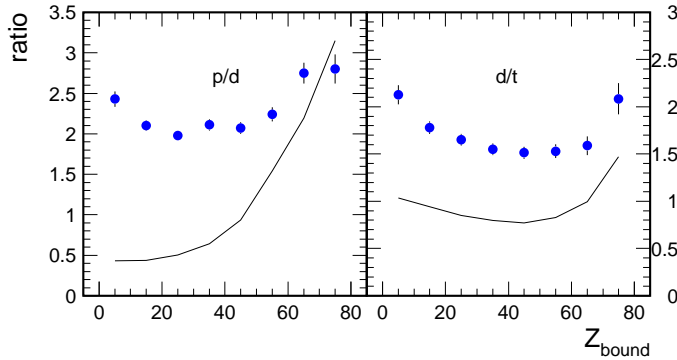


Figure 18: Proton to deuteron (left) and deuteron to triton ratios as function of Z_{bound} in the reaction Au+Au at 1A GeV. The experimental data are represented by data, statistical model calculations are given by the smooth lines. From ref. [8]

Can the clusterization in the fireball, Figs. 14, 15, also be understood in terms of chemical equilibrium? In view of the simple exponential shapes of the charge distributions, it does not come as a surprise that, given a fixed freeze-out density ρ , and the freedom to adjust the overall normalization, one can find an apparent chemical temperature T that reproduces the measured slopes well. The (ρ, T) pairs compatible with the FOPI data of Fig. 14 in the framework of the Quantum Statistical Model [16], QSM, are plotted in Fig. 19 adapted from ref. [12].

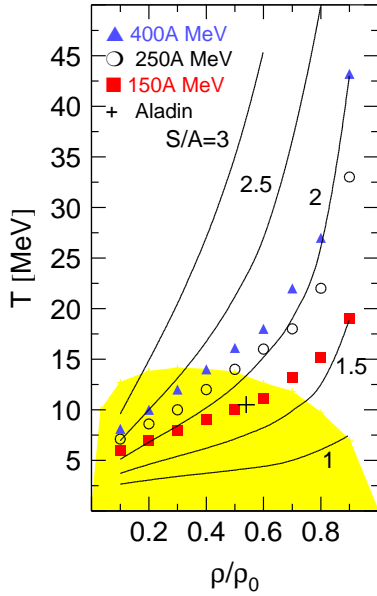


Figure 19: Temperature versus freeze-out density as determined from the comparison of the experimental charge distributions with those calculated with QSM for Au+Au at 150A, 250A and 400A MeV. Some isentropic curves (constant S/A) are also shown. [12] The shaded area represents the spinodal region. [17] Cross: inferred from adjacent Figure. See text.

As the (ρ, T) pairs run approximately along lines of constant specific entropy (S/A), one can use this kind of study to deduce the latter. [12] Just for the sake of orientation, the spinodal region, calculated [17] for isospin symmetric matter, is also indicated in the figure. Unless one allows for rather high freeze-out densities (such as $0.8\rho_0$), these apparent temperatures are rather low as we will see later.

Fireball matter was also studied in a Au on Au experiment with the ALADIN setup. [7] The temperature $T(\text{HeLi})$ is found to rise steadily with in-

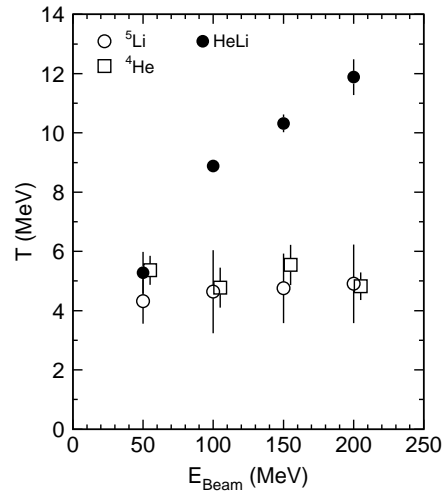


Figure 20: Temperature $T(\text{HeLi})$ (full symbols) and excited state temperatures (open symbols) as a function of incident energy per nucleon in Au on Au collisions. [7]

cident energy, Fig. 20, and is compatible with the FOPI results in Fig. 19 if the overlapping T(HeLi) point at 150A MeV (cross in Fig. 19) is inserted at a density close to $0.5\rho_0$.

Again, a warning is given by Nature: Temperatures deduced [7] from excited-state populations (^5Li , ^4He , ^8Be) seem to cluster around 5 MeV and are invariant against variation of the incident energy. See Fig. 20.

6 Peripheral collisions: Kinetic energies, calorimetry

The considerations in the previous section left out the information on momentum space distributions.

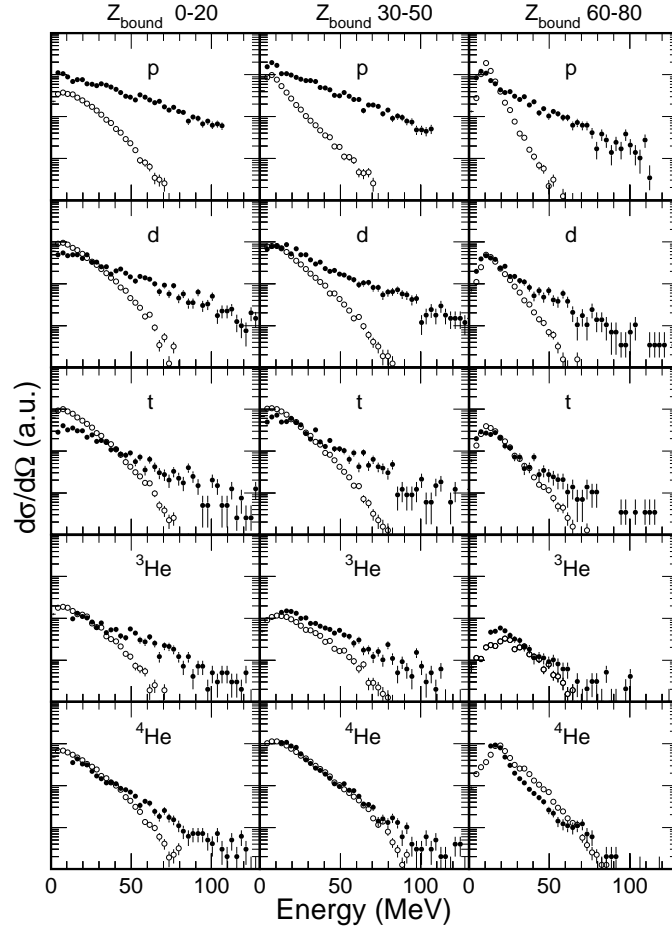


Figure 21: Energy spectra of light charged particles in three different bins of Z_{bound} . Solid dots: Experimental data obtained at 150° in the laboratory. Open symbols: SMM calculations. [8]

Figure 21 (light charged particles) and 22 (IMF's) summarize, for Au on Au at 1A GeV, the remarkable differences between the experimentally observed kinetic energies and the predictions of the statistical approach, that was adjusted to render correctly the yields of $Z > 2$ spectator fragments. Taking a closer look at Fig. 21 (the normalization of theory was done at the ${}^4\text{He}$ level, lowest panels), one notices that the deviations between theory and experiment increase from more peripheral (large Z_{bound} , right column) to more central collisions (left column) and decrease as the fragment mass is raised from $A = 1$ (top row) to $A = 4$ (bottom row). The average kinetic energies of the IMF's, Fig. 22, also follow a remarkable pattern that differs from the statistical-model calculation. The latter predicts a monotonic, slowly rising trend with nuclear charge, due to Coulomb effects.

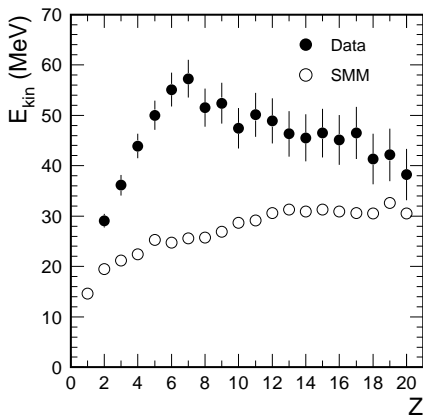


Figure 22: Average kinetic energies of spectator fragments as function of their charge in the reaction Au+Au at 1A GeV. Solid symbols: data, open symbols: SMM calculations. [8]

It has been argued [18] that such observations give strong evidence for a non-equilibrium situation, that can only be treated correctly by transport model approaches, such as Quantum Molecular Dynamics (QMD).[19] It was also proposed [8] that a sizeable part of the kinetic energy stems from fast freeze-out of Fermionic motion.[20]. Whatever the final explanation will be, such 'non-thermal' or 'non-classical' phenomena make the determination of the so-called caloric curve [3] i.e. a plot of the temperature versus the excitation energy per nucleon, very difficult. If such a curve, see Fig. 23, is to represent a state property of (finite) nuclear systems, perhaps suggesting by its plateau-like behaviour a liquid-to-gas transition, then it should be stable against the method applied. The major problem is to determine the abscissa which is usually obtained by the 'calorimetric' method, consisting essentially in adding up all the measured kinetic energies, perhaps with some high-energy tails cut off in a more or less well justified way. A preliminary result [8] obtained recently, Fig. 24, shows that the apparent plateau width depends on the incident energy.

Despite these unsolved problems in deriving a 'robust' caloric curve, it is highly interesting that theoretical approaches using fermionic dynamics [21, 22] predict caloric curves that have great similarity to the curve [3] presented in Fig. 23.

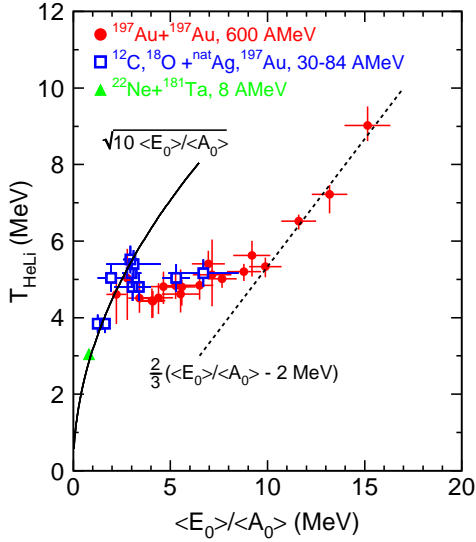


Figure 23: The caloric curve showing the dependence of the isotopic temperature on the excitation energy per nucleon. From ref. [3]

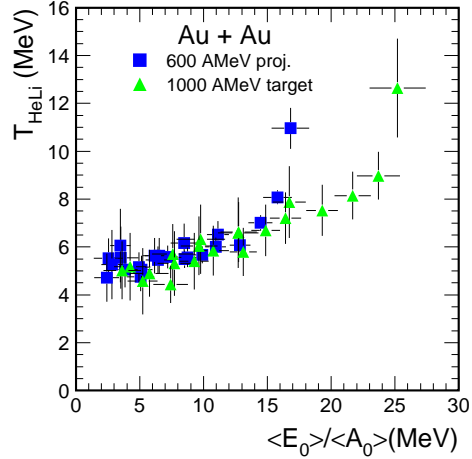


Figure 24: Comparison of the caloric curves obtained for Au+Au at 600A and 1000A MeV. From ref. [8]

7 Central collisions: Flow and system-size dependences

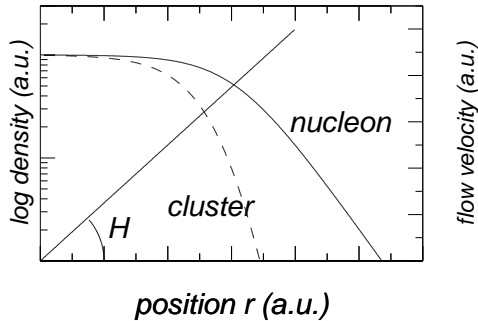


Figure 25: Freeze out profile (schematic): density and flow velocity (straight line)

ions (Fig. 26, left). A characteristic feature is that in contrast to a pure Boltzmann scenario (no flow) one sees curved mass dependent spectra. Those of heavier particles show a 'blueshift' in a spectacular way as they are less sen-

The fireball is not enclosed in a box (thermal model) but is expanding in much the same way as the universe. At freeze out the configuration of nucleons is expected to look roughly as shown in Fig. 25. There is a Woods-Saxon like density profile with a bulk part, having subsaturation density and an extended even lower-density surface part. Within the bulk part the flow velocity is rising linearly. With such a scenario, and assuming that the local temperatures are not varying much over the configuration, one can describe kinetic energy spectra [9] of emitted clustered nucleons

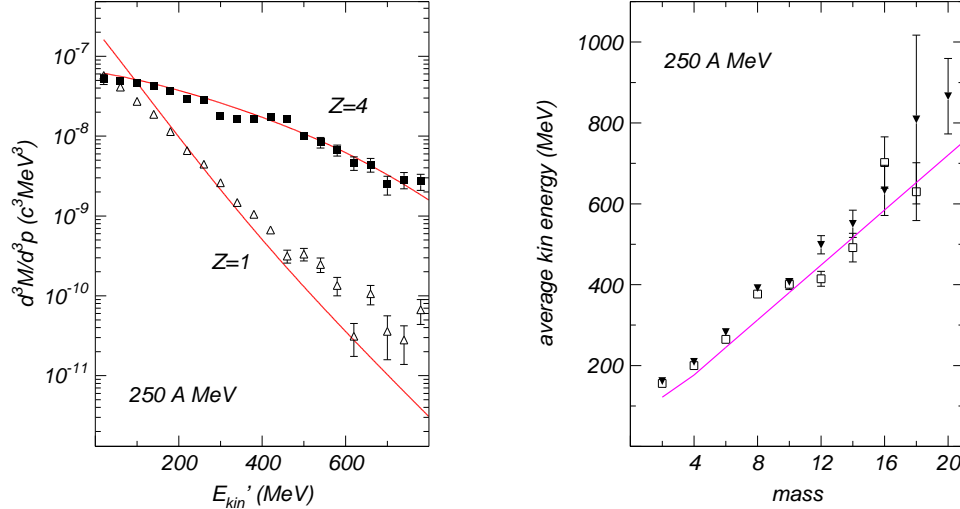


Figure 26: Left panel: Kinetic energy spectra of Z=1 and Z=4 fragments in central Au on Au collisions. Right panel: Mass dependence of average kinetic energies. The smooth curves in both panels are blast-model fits to the data.

sitive to thermal fluctuations that sit on top of the flow patterns and tend to wash out the flow features. Another way of showing evidence for radial flow are the mass-dependent average kinetic energies (Fig. 26, right). In a thermalized system enclosed in a box, rather than expanding, the kinetic energies should be independent on mass.

The energy taken up by such an expansive flow was estimated to be as high as 60%. [23, 9] At 250A MeV incident energy, to be specific, this still meant that about 20 MeV per nucleon (the Q-values are about $-5A$ MeV) were available for 'local use'. It is therefore not surprising that statistical multifragmentation calculations, allowing for the available *local* energy, still failed to reproduce the measured fragment yields as illustrated in Fig. 28. To obtain fair agreement with the data one has to assume that the primary fragments are cold [23], in contradiction to statistical expectations.

Transition to transport models, not limited by the local equilibrium assumption, seems mandatory. In the past the IQMD model calculations [19, 24] have been unable, though, to reproduce the observed IMF multiplicity, see Fig. 27. Modern developments are promising: a new cluster finding algorithm [25] seems to be successful.

One has tried to overcome the lack of quantum fluctuations in these quasi-classical simulations by introducing either so-called Quantum-Langevin methods [26] or by using Antisymmetrized Molecular Dynamics [27, 28].

In the following we discuss new, partially preliminary results obtained by

the FOPI Collaboration, that shed additional light onto this complex subject.

It is of high interest to study system size dependences. Are the fireball data as 'universal' as the 'spectator' data are? We have studied the number of

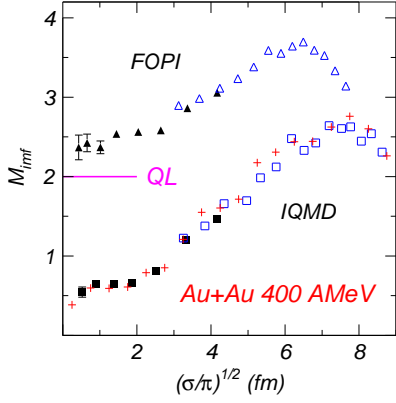


Figure 27: Impact parameter dependence of IMF multiplicities in experiment (triangles) and theory (IQMD, squares, Quantum-Langevin, QL, straight line).

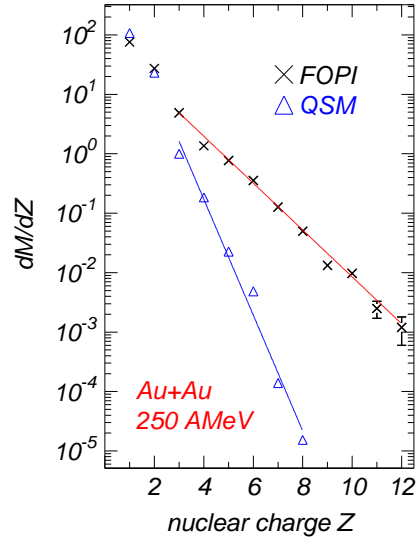


Figure 28: Comparison of experimental (FOPI) charge distributions with hydrothermal estimate

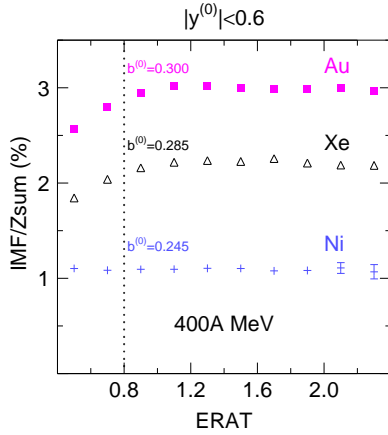


Figure 29: Normalized IMF ($Z > 2$) production in various indicated symmetric systems. The abscissa ERAT is the ratio of total transverse to longitudinal kinetic energy. Values in excess of 0.8 correspond to collisions with reduced impact parameter below 0.3.

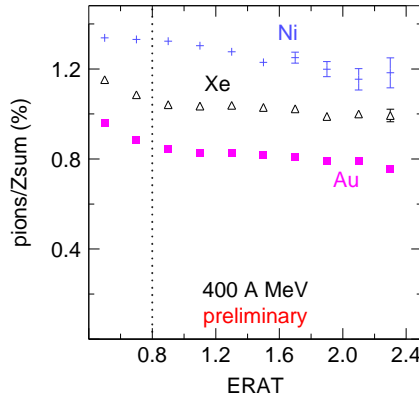


Figure 30: Same as adjacent figure, but for pions

emitted intermediate-mass fragments and the pion multiplicities varying the system size from $^{58}\text{Ni}+^{58}\text{Ni}$, via $^{129}\text{Xe}+\text{CsI}$ to Au+Au, see Figs. 29 and 30. Roughly, normalizing to a total of hundred observed baryonic charges, we find that three IMF are emitted in Au on Au reactions, two IMF in Xe+CsI and one IMF in Ni on Ni reactions. The order is inverted for pion emission: relatively more pions are emitted from the lighter Ni+Ni system (Fig. 30). Using thermal language, one might say that heavier systems appear to be cooler at freeze-out, perhaps favoured by a more substantial bulk expansion.

This seems to be corroborated by flow studies. Coming back to the directivity D introduced in section 2 to sort out very central collisions, we compare in Fig. 31 directivity distributions measured for Ni+Ni and Au+Au at 90 and 400A MeV. The reduced impact parameter range is $0 < b^{(0)} < 0.4$ (touching configurations corresponding to $b^{(0)} = 1$). The (two-dimensional) random walk distributions of D (crosses), obtained by randomizing the azimuthal emission angles in each event, are compared with the actual distributions (histograms).

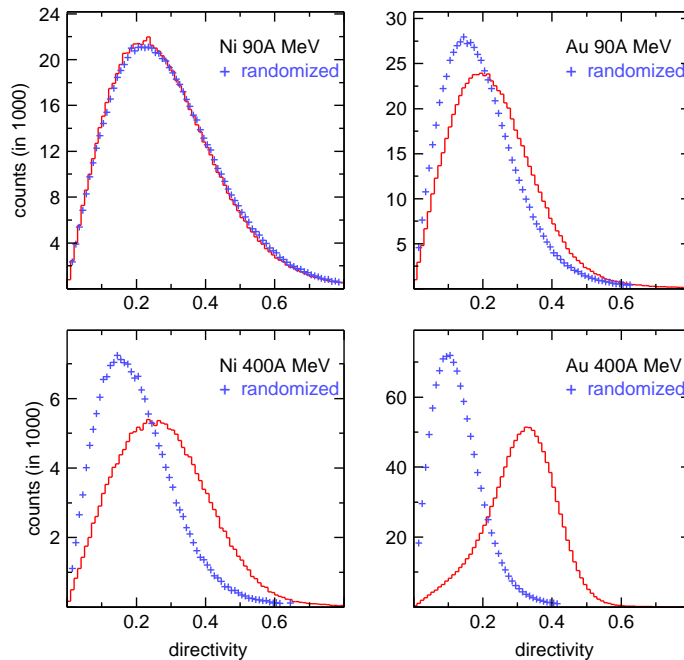


Figure 31: Directivity distributions in various indicated systems at the same normalized centrality. The signal (histogram) is compared to distributions from azimuthally randomized events.

One finds that the random distributions of this scale-invariant observable are broader for lighter than heavier systems (i.e. the *relative* fluctuations are larger), see the top two panels in Fig. 31, and narrow down at higher energies

because of increasing particle multiplicities (compare the top with the bottom panels). Comparing with the actual distributions one sees that

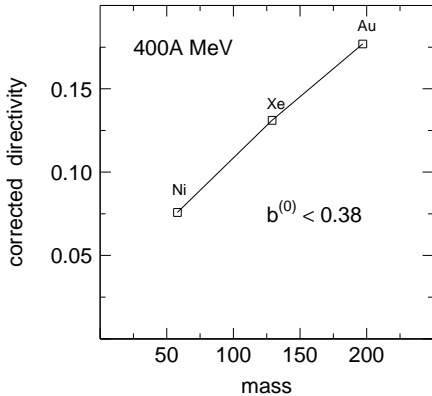


Figure 32: Corrected directivity versus projectile mass in symmetric systems at 400A MeV beam energy

well require the consideration of fast non-equilibrium mechanisms, as proposed elsewhere [29] in a different context. The very low 'temperatures' suggested by the analyses [12, 7], see Figs. 19, 20, would then be an artifact of an inadequate assumption (equilibrium).

8 Non-equilibrium: isospin tracer method

Valuable insight into the question of equilibration can be gained by studying systems, that, while mass symmetric, are isospin asymmetric. We have performed an 'isospin tracer experiment' using four mass 96+96 systems Ru+Ru, Zr+Zr, Ru+Zr and Zr+Ru at 400A MeV. Naively, if Ru was to impinge on Zr, then, after the collision and in the case of complete transparency, we should be able to count 44 protons (Ru) in the forward rapidity hemisphere, and we should find the 40 protons of Zr at backward rapidities. In the extreme limit of a *collective* 'rebound' (predicted by one-fluid non-viscous hydrodynamics, as we shall see), just the opposite would be observed, while 'complete mixing' would show up as a 'white' distribution.

A more complete description of this experiment is given in reference. [30] In the studied reactions, if central collisions are selected, the transverse-momentum vs rapidity distributions of emitted protons indicate the apparent dominance of *one* nearly isotropic source located at midrapidity. Fig. 33 shows for very central collisions the result of 'proton-counting' (including those in

- 1) At 90A MeV there is no net effect for the Ni system, while a statistically significant signal is seen for Au.
- 2) At 400A MeV sideflow has increased substantially in both systems.
- 3) The sideflow, Fig. 32, after correction for the finite number fluctuation, shows a dramatic system-size dependence.

We are currently also studying other aspects of flow, such as radial flow and out-of-plane flow as a function of system size. It is intriguing to connect information on flow with the probability to form clusters. The failure of the hydrothermal attempt to understand the degree of clusterization, Fig. 28, suggests that rapid expansion physics may

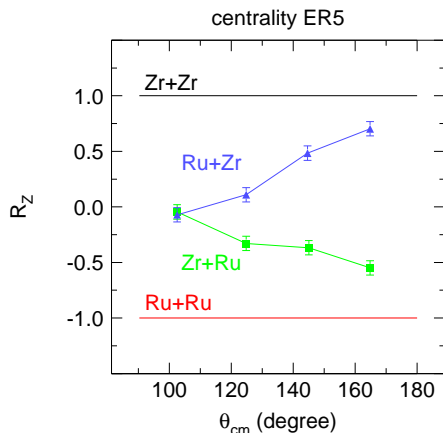


Figure 33: Proton counting as a function of polar angle in four mass-96 on mass-96 systems at 400A MeV (see text).

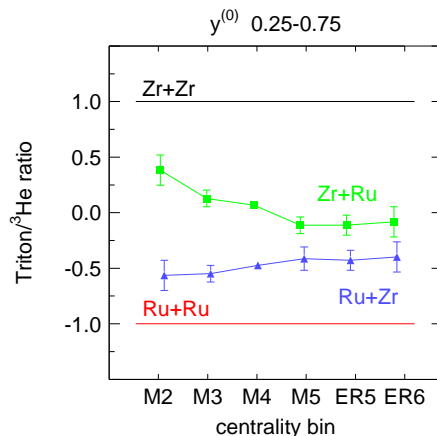


Figure 34: Normalized triton/ ^3He ratios as a function of centrality

deuterons) for the four systems as a function of the center-of-mass polar angle. To quantify conveniently the 'degree of mixing' we first study the symmetric systems Ru+Ru and Zr+Zr and renormalize in each angular bin the observable to $+1$ (Zr), resp. -1 (Ru). Using this normalization, we then study the asymmetric systems $\text{Ru} \rightarrow \text{Zr}$ and the 'inverse' reaction $\text{Zr} \rightarrow \text{Ru}$. As can be seen, the two asymmetric systems converge to the expected mixed value (zero) only near 90° , where they *must* converge. As soon as one leaves the 90° interval, the proton counting observable tends to the value expected for transparency, the sign being opposite for the Ru+Zr and Zr+Ru systems, as it should be for internal consistency.

An alternative way of demonstrating this partial transparency is to use instead the triton to ^3He ratio (Fig. 34). Again one proceeds by looking at the symmetric system first, normalizes the difference to ± 1 and then studies the asymmetric systems. This time we fix the phase-space region: we look at to $y^{(0)} = 0.25 - 0.75$. We now vary the centrality from impact parameters below 1 fm (ER6) to about 8 fm (M2). Note again that effects can only be expected away from midrapidity. We find that our second observable again indicates partial transparency, although the effect is least pronounced for the most central collisions. One can show by the way [32] that the 'fully mixed' value should be somewhat below the zero line in Fig. 34, near (-0.20) .

If one uses the proton-counting method as a function of rapidity, rather than polar angle as was done in Fig. 33, one can actually decompose the rapidity distribution in a projectile and a target 'remnant', as shown in Fig. 35.

What can we conclude? We believe these types of data are important for

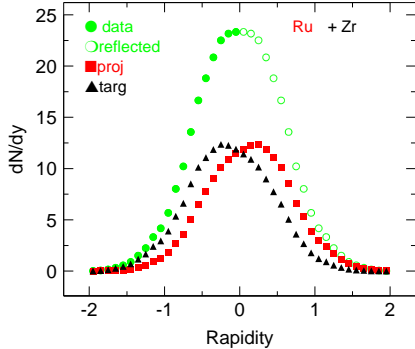


Figure 35: Decomposition of the rapidity distribution in central collisions of $^{96}\text{Ru} + ^{96}\text{Zr}$ at 400A MeV. After ref. [30]

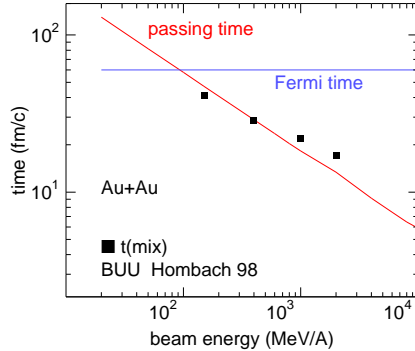


Figure 36: Passing time, Fermi time and mixing time (symbols) as a function of beam energy

at least two reasons.

1) it is good to have a signature of partial memory of the past: this puts a constraint on dynamic models; these models must show that they can realistically cope with the observed partial transparency, independently whether its origin is connected with the surface corona and possibly even with insufficient stopping volume. Reactions with heavy ions *always* concern finite sizes and corona effects.

2) If the system is not fully equilibrated at the *end* of the evolution, we expect it to be even less equilibrated at earlier stages, i.e. at maximum compression. Hence the pressure expected from the nuclear equation of state (EOS) is not fully developed, which in turn will lead to decreased flow at the end of the evolution. *Transparency may mock up a 'soft' EOS.* Transport models used to extract information on the EOS must therefore correctly reproduce the observed partial transparency (be it bulk and/or surface transparency).

Clearly, corona effects must be one of the reasons for observing partial transparency, although they are subtle: for the most central collisions they do not appear as an obvious structure close to target or projectile rapidity (see Fig. 35). Various transport calculations shedding light on the mixing problem have already been done. In Fig. 36 we show results deduced from recent work of Hombach et al.[31]. Using a periodic box condition the authors have determined the equilibration time for nucleon mixing in the SIS energy range. They find times on the order of 40 to 10 fm/c decreasing with increasing incident energy (see the Figure).

Comparing this with the passing time ($2R/u$) (R projectile radius, u four-velocity), and the Fermi-time (typical time for a nucleon to cross the system due to its Fermi-motion), we can conclude from this study that the passing time might be somewhat too short for equilibration below 500A MeV. The

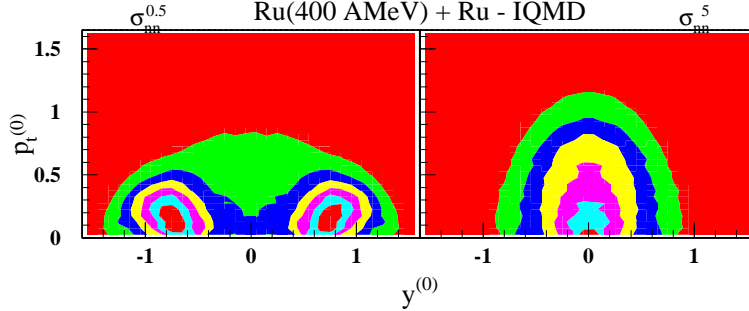


Figure 37: Momentum space distributions in a transparency and a hydro-shock scenario.

relative transparency at lower energies is intimately connected with the importance of Pauli blocking and the still frozen nucleonic degrees of freedom. (The mobility implied by the Fermi time is important for the communication between 'participants' and 'spectators').

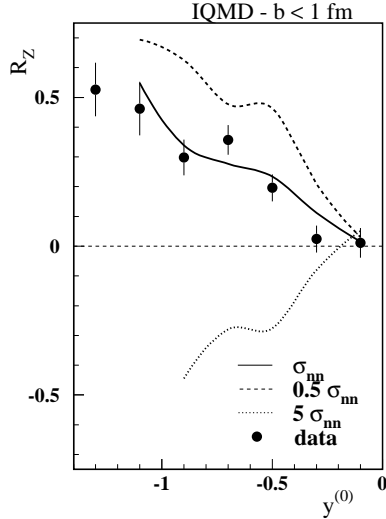


Figure 38: Comparison of the proton counting observable with various IQMD simulations

experiment. In the latter case, almost instant equilibration leads to highly oblate event shapes with increased particle emission at 90° (c.o.m.): the true 'squeeze-out' predicted in the early seventies [33]. The consequences for our proton counting observable are seen in Fig. 38. In particular the hydro-shock scenario leads to a rebound, the opposite of what we observe. The data are in between the two scenarios (although closer to the 'transparent' scenario)

Transparency is sensitive to the medium-modified nucleon-nucleon elastic scattering cross sections σ_{nn} . Fig. 37 shows momentum-space distributions for Ru+Ru at 400 AMeV obtained using the IQMD transport code [24] with two extreme, but instructive, assumptions: for the left panel we used [32] $0.5 * \sigma_{nn}$ and for the right panel $5 * \sigma_{nn}$ (σ_{nn} are free-scattering cross sections from the literature). We note that the code of course applies the usual Pauli-blocking weights in the collision term [19]. This takes care of some, but not all in-medium effects. The two (impact parameter zero) cases illustrate the transparent and the 'hydro-shock' alternatives. In the former case one still sees 'spectator' sources, in contrast to ex-

and are in impressive agreement with IQMD predictions using the nominal σ_{nn} (solid curve). It is important to realize that only a *fraction* of the flow-creating pressure expected from ideal hydrodynamics is achieved in a heavy ion collision.

9 Conclusion

We have presented multifragmentation data from heavy ion reactions at incident energies varying from 0.1A to 1A GeV. Two powerful and to some degree complementary experimental setups, ALADIN and FOPI, allowed us to study the complex decay of both 'spectator' and 'fireball' or 'participant' matter. It appears that rather different mechanisms govern these multiparticle events. While a remarkable 'universality', i.e. invariance under variation of the system size and of the incident energy, was seen to characterize the decay of the intermediate mass fragment source in the case of spectator matter, we saw that in contrast, the decay of rapidly expanding fireball matter showed pronounced system-size dependence, that could be traced, at least in part, to the occurrence of significant size-dependent flow.

Purely statistical concepts, comparatively successful in explaining the yields of particles with $Z > 2$, fail when it comes to explaining light particle yields, and above all when momentum space distributions are to be understood. Even the 'universal' spectator decays are accompanied by an apparently fast removal of some of the available energy primarily by single nucleons and show a non-trivial evolution of average kinetic energies with the nuclear charge, implying the presence of either flow (sideways bounce or radial) or fast freeze-out of Fermionic motion, possibly due to large scale fluctuations caused by the system passing through the spinodal region, or some entrance-channel memory effects.

Such phenomena must be understood before we can think of deriving a 'robust' caloric curve for finite nuclei, that we eventually could extrapolate to infinite nuclear matter.

It seems also urgent to join up the 'spectator' data with information from lower energy reactions, both central (one-source) and peripheral (quasiprojectile). Evidence for a liquid-gas transition has been claimed recently for quasiprojectile decay, [34] as well as spectator decay. [3, 35]

The mechanisms of multifragmentation in an expanding fireball are not yet fully understood. The underestimation of the degree of clusterization in a hydrodynamic scenario with *local* equilibration, the observed system-size dependences and the lack of complete isospin-mixing indicate that fast expansion physics maybe a non-equilibrium process. While the role of flow seems qualitatively evident, the quantitative connection to the Equation of State must be further explored.

New isospin-tracing experiments have a potential to overcome some of the

questions relating to a *quantitative* assessment of non-equilibrium features.

The fact that we observe the clusterization of finite pieces of fermionic matter in at least a partially non-equilibrated environment calls for application and the further development of *quantum* transport theories, that fulfill in the static limit the well known requirements of *nuclear* physics theory.

Acknowledgements

The data and ideas presented here are the result of the coordinated work of two large Collaborations. I owe special thanks to W. Trautmann for his generous help and advice concerning the presentation of the ALADIN data.

References

- [1] H. Feldmeier, J. Knoll, W. Nörenberg, J. Wambach (Eds.), *Multifragmentation. Proceedings of the International Workshop XXVII*, Hirschegg, Austria, Jan. 17-23, 1999; GSI, Darmstadt, Germany 1999, ISSN 0720-8715.
- [2] P. Kreutz et al. , Nucl. Phys. **A556** (1993) 672.
- [3] J. Pochodzalla et al. , Phys. Rev. Lett. **75** (1995) 1040.
- [4] A. Schüttauf et al. , Nucl. Phys. **A607** (1996) 457.
- [5] Hongfei Xi et al. , Z. Phys. **A359** (1997) 397.
- [6] M. Begemann-Blaich et al., Phys. Rev. **C58** (1998), 1639.
- [7] V. Serfling et al. , Phys. Rev. Lett. **80** (1998) 3928.
- [8] T. Odeh , PhD Thesis, University Frankfurt, 1999; GSI Rep. Diss. 99-15 , 1999.
- [9] W. Reisdorf et al. , Nucl. Phys. **A612** (1997) 493.
- [10] M.F. Rivet et al. , Phys. Lett. **B430** (1998) 217.
- [11] L. Beaulieu et al. , Phys. Rev. **C54** (1996), R973.
- [12] C. Kuhn et al. , Phys. Rev. **C48** (1993), 1232.
- [13] J.P. Bondorf, A.S. Botvina, A.S.Iljinov, I.N. Mishustin, K. Sneppen. Phys. Rep. **257** (1995), 133.
- [14] A.S. Botvina, I.N. Mishustin, et al. , Nucl. Phys. **A584** (1995) 737.

- [15] S. Albergo, S. Costa, E. Costanzo, A. Rubbino, *Il Nuovo Cimento* **89A** (1985) 1.
- [16] D. Hahn, H. Stöcker, *Phys. Rev.* **C37** (1988), 1048.
- [17] H. Müller, B.D. Serot, *Phys. Rev.* **C52** (1995), 2072.
- [18] P.B. Gossiaux, R. Puri, Ch. Hartnack, J. Aichelin, *Nucl. Phys.* **A619** (1997) 379.
- [19] J. Aichelin, *Phys. Rep.* **202** (1991) 233.
- [20] W. Bauer, *Phys. Rev.* **C51** (1995), 803.
- [21] J. Schnack, H. Feldmeier, *Phys. Lett.* **B409** (1997) 6.
- [22] Yoshio Sugawa, Hisashi Horiuchi *Phys. Rev.* **C60** (1999), 064607.
- [23] M. Petrovici et al. , *Phys. Rev. Lett.* **74** (1995) 5001.
- [24] Ch. Hartnack, PhD Thesis, University Frankfurt, 1993; GSI Rep. 93-5 , 1993 (in German).
- [25] R. Nebauer, A. Guertin,R. Puri, Ch. Hartnack,P.B. Gossiaux, J. Aichelin, see ref. 1,p.43.
- [26] A. Ohnishi, J. Randrup, *Phys. Lett.* **B394** (1997) 260.
- [27] H. Feldmeier, *Nucl. Phys.* **A514** (1990) 322.
- [28] A. Ono, H. Horiuchi, T. Maruyama, A. Ohnishi, *Prog. Theor. Phys.* **87** (1992), 1185.
A. Ono, *Phys. Rev.* **C59** (1999), 853.
- [29] B.L. Holian, D.E. Grady, *Phys. Rev. Lett.* **60** (1988) 1355.
- [30] F. Rami et al. , *Phys. Rev. Lett.* **84** (2000) 1120.
- [31] A. Hombach, W. Cassing, U. Mosel, *Eur. Phys. J.* **A5** (1999) 77.
- [32] B. de Schauenburg, PhD Thesis, University Strasbourg 1999.
- [33] W. Scheid, H. Müller, W. Greiner, *Phys. Rev. Lett.* **32** (1974) 741.
- [34] M. D'Agostino, et al., *Nucl. Phys.* **A650** (1999) 329 and *Phys. Lett.* **B473** (2000) 219.
- [35] J.B. Elliott, et al., *Phys. Lett.* **B418** (1998) 34 and references therein..